JOURNAL OF MATERIALS SCIENCE 8 (1973) 59–70

Hydrostatically-extruded polypropylene

T. WILLIAMS
ICI Corporate Laboratory, Runcorn, Cheshire, UK

Melt-extruded cylinders of polypropylene can be hydrostatically extruded in the solid-phase to give uniform, highly-oriented rods. The tensile and torsional moduli of such extrudate have been measured as a function of the amount of deformation. Values obtained after large deformations are greater than those previously observed for drawn fibres. Birefringence and X-ray diffraction measurements of orientation have been compared and used to assess uniformity, and to predict the moduli on the basis of a simple aggregate model. Although the changes in modulus at low deformation ratio were not inconsistent with the model, there is definite evidence that it is not applicable to highly-deformed samples.

1. Introduction

The structure and mechanical properties of polymers are considerably modified by a deformation process such as cold-drawing or rolling. Molecules are aligned along the extension direction and there can be a large increase in stiffness and strength in that direction. The improvements in tensile properties have been exploited for many years in polymer fibres and films. Despite this vast commercial exploitation, the precise structural changes occurring during deformation and the relationship between the structural changes and mechanical properties of the oriented polymer are still a subject of some controversy.

In isotropic, melt-crystallized polymers it is generally recognized that the crystalline units are lamellar with lateral dimensions much larger than their thickness. The molecules are usually oriented near to the perpendicular to the large surfaces of each crystal and it is thought that some fold back into the same crystal at the large surfaces, whilst others pass into disordered intercrystalline regions and then possibly into other crystalline regions. The crystalline units themselves are usually aggregated into spherulites [1].

When a polymer sample is drawn, it often deforms inhomogeneously and a necked region, consisting of highly-oriented polymer, forms whilst most of the material is only slightly oriented. With increased extension, the highly-oriented, yielded region usually spreads along the sample at the expense of the slightly-oriented material. In other cases, the sample deforms more uniformly up to its maximum draw ratio at which point fracture occurs. Each of these two types of deformation will involve some re-orientation of the basic crystalline units. There is probably, in addition, some fragmentation of the crystals to form crystal blocks of smaller width [2]. It has even been suggested that there is complete fragmentation ("local melting") of crystals, with recrystallization to form the structure of the drawn fibre. The extent of crystal fragmentation during re-orientation could depend upon the amount and size of crystalline material in the original sample and also the deformation conditions [1].

If the polymer is assumed to consist of units which simply become oriented during deformation, the polymer properties can be deduced in terms of the properties assumed for the individual units and the orientation distribution of the units [3]. This "aggregate model" accurately predicts the changes in elastic moduli which occur upon deforming low density polyethylene [4] and polyethylene terephthalate [5]. It does not, however, successfully predict the modulus changes for more crystalline polypropylene fibres [6].

A free-drawing process cannot be used to produce oriented polymer samples of more

massive section than fibres and films because the process is not controlled and "necking" usually occurs. This produces material which has non-uniform cross-section and deformation. In an attempt to produce oriented polymer rods with uniform cross-section a research project was established to investigate the application to thermoplastics of the metal-working technique solid-phase hydrostatic extrusion [7]. During this process, a solid cylindrical billet of material is forced through a die by hydrostatic pressure transmitted to it via a surrounding liquid. The shape and size of the extrudate is determined by the die. Large cross-sections of controlled, complicated shape can be obtained. In metal technology, the process is used for shaping, whereas our work with polymers was primarily interested in the process for tensile property improvement as a result of orientation.

During comprehensive research into solid-phase hydrostatic extrusion, the processing of several different polymers was studied. These included polypropylene, low- and high-density polyethylene, polyethylene terephthalate, nylon 6,6, polymethyl methacrylate and polyvinyl chloride. All polymers gave extrudate with an excellent smooth surface finish. As expected [8] greatest anisotropy was developed for the crystalline polymers. One such polymer which was found particularly easy to process was polypropylene. Most detailed measurements were therefore confined to this polymer and it is these measurements which are reported in this paper.

2. Theory

2.1. Orientation measurements

The birefringence of a partially-oriented polymer indicates the extent of molecular orientation. If the sample is considered to consist of units of intrinsic birefringence Δn_m then with increase in the orientation of the units from a random distribution, the sample birefringence Δn will increase from zero up to the maximum birefringence Δn_m. If θ is the angle of any unit to the deformation direction, then

$$\Delta n = \Delta n_m(1 - (3/2)\overline{\sin^2\theta}) \text{ (see [3])} \quad (1)$$

Now all molecular segments in the sample influence the birefringence. Hence the orientation function $\overline{\sin^2\theta}$ gives an overall average orientation function for molecules in crystalline and non-crystalline regions.

Other orientation functions can be defined from X-ray diffraction measurements. The intensity of X-rays diffracted from crystal planes is measured as a function of the angle to the deformation direction. Hence the relative numbers of planes oriented in each direction in the sample can be measured and average orientation functions, $\overline{\sin^2\theta}$, $\overline{\sin^4\theta}$ etc, for the normals to the selected planes can be calculated. For planes perpendicular to the c-axis of the crystal, the orientation functions indicate directly the molecular orientation in the crystal. Unfortunately for polypropylene, there are no crystal planes perpendicular to the c-axis which diffract X-rays. Hence the orientation functions for the crystal c-axes cannot be determined directly from a single intensity scan. They can however be calculated from the intensity distribution of radiation scattered from two sets of crystal planes, both of which contain the c-axis [9]. Elaboration of the theory behind this technique is contained in the Appendix.

If deformation occurs with no change in volume and molecular segments are aligned at the same rate as macroscopic lines connecting different points in the sample, then an average orientation function $\overline{\sin^2\theta}$ for all molecular segments can be related to the deformation ratio R:

$$\overline{\sin^2\theta} = \frac{K}{(1 - K^2)^{3/2}} [\cos^{-1}K - K(1 - K^2)^{1/2}] \quad (2)$$

where $K = R^{-3/2}$. This is called pseudo-affine deformation [3].

2.2. The aggregate model

The aggregate model [3] predicts the elastic moduli of a partially-oriented, transversely-isotropic polymer. In the model, the polymer is considered to consist of transversely isotropic units of structure, each of which has the properties of the fully extended fibre. As a result of the drawing process, the units of structure are re-oriented towards the draw direction. With a given orientation distribution, the moduli of the units can be averaged to give the moduli of the polymer sample. In the averaging procedure it is necessary to assume that either the stress or the strain is the same in each unit. These assumptions give two limiting bounds (the Reuss and Voigt bounds respectively).

It has been shown that the Reuss (lower) bound gives the better fit to polymeric behaviour. This bound involves the averaging of compliance constants and these are more easily determined from experimental measurements. It predicts

that the extensional compliance along the draw direction S_{33}' and the torsional compliance S_{44}' of the aggregate are given by:

$$S_{33}' = \overline{\sin^4\theta}\, S_{11} + \overline{\cos^4\theta}\, S_{33} + \overline{\sin^2\theta\cos^2\theta}\,(2S_{13} + S_{44}) \quad (3)$$

$$S_{44}' = (\overline{\sin^2\theta} + 2\,\overline{\sin^2\theta\cos^2\theta})\, S_{11} - \overline{\sin^2\theta}\, S_{12} + 2\,\overline{\sin^2\theta\cos^2\theta}\,(S_{33} - 2S_{13}) + (2 - \overline{\sin^2\theta} - 4\,\overline{\sin^2\theta\cos^2\theta})\, S_{44}/2 \quad (4)$$

where θ is the angle of the axis of a unit to the deformation direction and S_{11}, S_{12}, etc. are the compliance constants of the units.

The Voigt (upper bound) relates the stiffness constants of the aggregate to those of the units by equations similar to Equations 3 and 4. To test the model it is first necessary to predict the stiffness constants of a unit of structure. This can be done using matrix inversion formulae and previously-determined compliance constants. To compare predicted aggregate stiffnesses with experiment it is again necessary to use matrix inversion formulae to obtain the equivalent compliances which relate directly to experimental measurements.

3. Experimental details

3.1. The hydrostatic extrusion process

Solid cylindrical billets of undrawn polymer are necessary for the process. Most work was carried out using commercially-available, melt-extruded rods of Hoechst Chemicals grade PPH 6065 polypropylene. Molecular orientation was just detectable in these rods, the birefringence being 0.001. This is negligible compared to the orientation achieved by the process, a typical extrudate birefringence being 0.030. In preparation for hydrostatic extrusion a cone with the same angle as the die was machined at one end of the polymer rod.

Solid phase extrusion was carried out in a rod-spinner apparatus. The principle of operation is evident from Fig. 1. A plunger was forced by a ram down a barrel containing the billet and hydraulic fluid. The machined end of the billet sealed the hole in an extrusion die which was attached to the end of the barrel. Pressure was transmitted from the plunger to the fluid and forced the billet through the extrusion die. As well as transmitting pressure, it was found that the fluid lubricated the billet at the die and helped give the extrudate a very smooth surface finish. This contrasts with our efforts at dry ram extrusion which gave a product with a very rough surface texture [10]. For the experiments described herein, ICI Silicone Oil F111/300 was used as the hydraulic fluid together with an extrusion die with cone angle of 30° and aperture diameter 0.3 in. Extrusion was carried out at a temperature of 100° C.

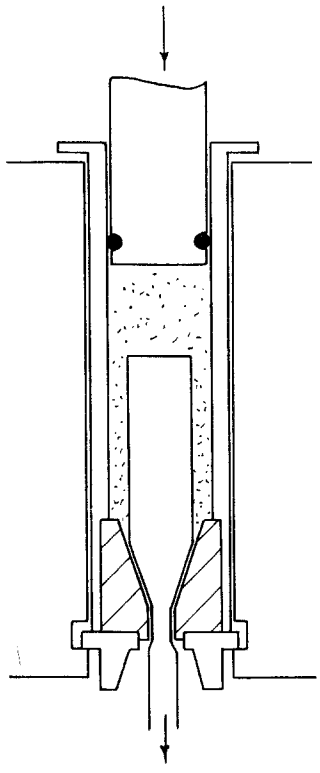

Figure 1 Hydrostatic extrusion apparatus.

After starting the downward motion of the ram, an increase in pressure was observed. At a critical pressure the material yielded and extrusion commenced. As soon as this occurred, a sudden decrease in pressure took place and steady extrusion occurred at a lower pressure. Typical hydrostatic pressures were in the range 5000 to 15000 psi. The value was found to be highly dependent on the polymer species, temperature and the amount of deformation attempted [10]. As the extrudate started emerging from the die, a weight (typically 700 g) was clamped to it. This tensile stress kept the extrudate straight.

The amount by which the billet was deformed during the process can be defined by the ratio of the areas of the original billet and the final extrudate. This deformation ratio was adjusted by machining the original billets to different initial diameters. Using the initial billet diameter

as the only variable it was found to be impossible to achieve a deformation ratio greater than 5. When larger ratios were attempted, the extrudate relaxed after emergence from the die and the final diameter was such that R was smaller than 5. This difficulty was overcome, however, by increasing the tensile force on the emerging extrudate to a sufficient level to eliminate relaxation. Typical weights required were in the range 80 to 130 kg. In this manner, deformation ratios up to a value of 15 could be obtained.

Much more detailed discussion of the process and the effect of variables such as die geometry and size will be made in a separate publication [10].

3.2. Tensile modulus measurements

Tensile properties were determined at room temperature at a constant strain-rate of $7\,\%\,min^{-1}$ using a Hounsfield tensometer. During the test, the extrudate was held by self-gripping jaws. Sample extension was measured using a 2 in. gauge length extensometer clamped to the sample. The output was fed to the x-axis of an x-y recorder. The output of the load cell was fed to the y-axis and thus a force-extension curve was plotted directly during the test. The secant modulus at 0.2 % strain was taken as a measure of the tensile modulus.

3.3. Birefringence measurements

A Zeiss Ultraphot-2 polarizing microscope was used to measure the birefringence of thin sections of extrudate. The conventional way of obtaining the thin sections necessary for birefringence measurements is to cut strips using a microtome. This technique was found to give highly variable results due to relaxation of the sections during or immediately after sectioning. Relaxation was evident since sections were shorter than the rod from which they were cut. It was therefore necessary to mill the cylindrical extrudate down from two directions to give a flat section. When the section thickness was smaller than 1 mm, variable results were again obtained, presumably due to machining effects on the sample. The limited travel of the compensator meant that for our samples, thicknesses larger than 2 mm could not be used. However, for thicknesses in the range 1 to 2 mm, results from neighbouring sections of extrudate were reproducible to within $\pm 3\,\%$, the expected tolerance of the measurements. Such samples were used for all of the birefringence data quoted.

3.4. Wide-angle X-ray diffraction

Qualitative information concerning the orientation of molecules in the crystalline regions of the samples were obtained using conventional wide-angle X-ray diffraction.

Quantitative measurements were made using a Siemens Texture Diffractometer [11]. This instrument can be used to automatically map out the pole figures of crystalline material. Full pole figures were constructed in the conventional manner for a few samples of extruded polypropylene and these confirmed that as might be expected from the geometry of the deformation, the samples were transversely isotropic. Hence complete quantitative information of the orientation distribution in each sample can be obtained by scans at constant diffraction angle. A transmission technique was used since, with this technique, no correction is required for changes in absorption with rotation of the sample (this fact was checked using an isotropic melt-pressed polypropylene sheet). For measurements on extruded polypropylene, milled sections of 2 mm thickness were used. The baselines of the intensity scans were determined for each sample with the analyser of the diffractometer set at 2° away from the diffraction angle.

4. Results and discussion

4.1. Flow pattern and uniformity of extrudate

From the nature of the deformation, it might be thought that there would be some variation in orientation, and hence mechanical properties, across the extrudate cross-section. This was checked using birefringence as a measure of the orientation. Surprisingly, no variation in birefringence could be detected across the entire width of a section. Now the volume sampled in each birefringence measurement is a cylinder of $\frac{1}{2}$ mm radius and 2 mm length. Thus any variation must be fluctuations occurring on a scale much smaller than 1 mm or be smaller than the possible error in birefringence measurements of $\pm 3\,\%$. The uniformity in orientation implies that all parts of the original billet undergo similar deformations in the extrusion process. This has been demonstrated by Cassin [10] using split gridded billets to map out the manner in which deformation occurred. A typical diagram of the flow pattern they observed during deformation is contained in Fig. 2.

A few experiments have been carried out using dies which produce non-circular cross-section extrudate. Other extrusion conditions were

identical to those described earlier. One die employed deformed circular cross-section billets to I-section extrudate. Much more complicated flow patterns are involved than with the radially-symmetric case of extrusion of one cylinder into another concentric one. Even for this complicated extrusion, however, the extrudate was found to be surprisingly uniform. The total spread in birefringence was 10% with the largest orientation in the flanges.

The tendency for the process to give uniform deformation across the entire section is probably due to the increase in stiffness of the material with increased deformation. Thus the change in properties of one element as a result of its deformation make it less amenable to further deformation. Hence extra load is placed on neighbouring elements until they too have been deformed to give the same change in properties.

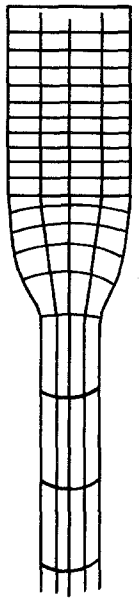

Figure 2 Gridded billet showing flow pattern during hydrostatic extrusion (after Cassin [10]).

4.2. Birefringence measurements

The birefringence induced in the extrudate as a result of solid-phase extrusion increases with increase in the deformation ratio. In Fig. 3, the increase is compared to that expected on the basis of pseudo-affine deformation (Equations 1 and 2 above). A value of 0.036 was used in Equation 1 for Δn_m since this empirical value gave agreement between the theoretical and experimental curves at large deformation ratios. At small deformation ratios the actual birefringence was always smaller than that predicted theoretically. The orientation therefore occurs more slowly than predicted by an affine deformation model. It also occurs more slowly than during cold-drawing of polypropylene fibres [6] for which a similar discrepancy between theory and experiment was observed. For polypropylene fibres a fit to the affine deformation theory was obtained when a "theoretical" deformation ratio R_T was used in Equation 2 instead of the true value R. In that case, R_T was found to be related to R by the equation:

$$\log R_T = (R - 1)/6.44$$

A similar form of empirical adjustment also gives a better fit in the case of hydrostatically-extruded polypropylene (see Fig. 4). In this case the best agreement was obtained using an equation:

$$\log R_T = (R - 1)/8.4$$

A departure from the new theoretical/empirical curve is still evident at large deformation ratios. No such departure was detected in the previous work with fibres.

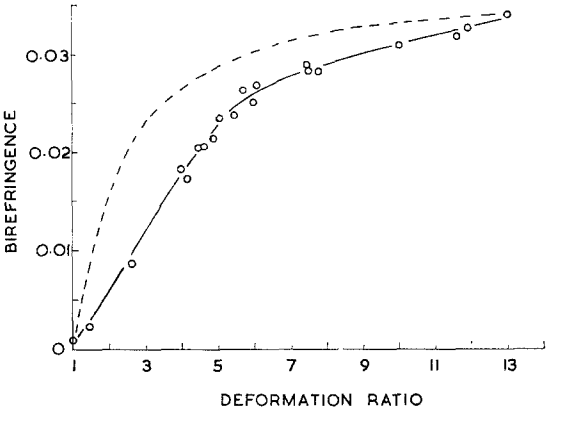

Figure 3 Variation of birefringence with deformation ratio. The dotted curve is the theoretical curve deduced assuming affine deformation.

4.3. Wide-angle X-ray diffraction

The manner in which the orientation of the crystalline regions develops is indicated qualitatively by wide-angle X-ray diffraction. The original billet has a diffraction pattern consisting of concentric rings (Fig. 5a), i.e. the intensity of diffracted radiation from each set of atomic planes is independent of the rotation of the

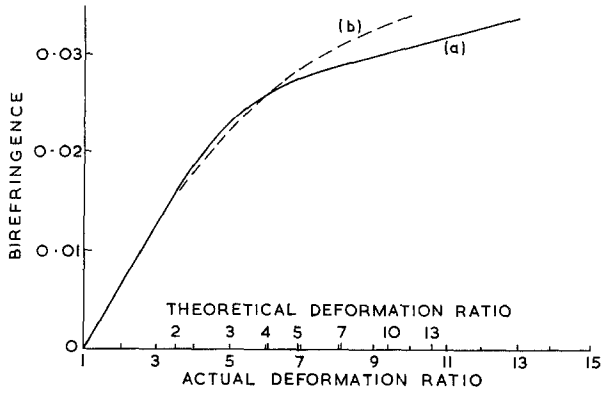

Figure 4 Comparison of the increase in birefringence upon deformation (a) with an affine deformation model after empirical adjustment of the deformation ratio scale (b).

sample. This indicates that the billets are essentially isotropic. (In fact, the outer rings of Fig. 5a are oval and not circular because, for this qualitative work, a cylindrical plate was used.) After the largest deformation ratios, each reflection is confined to vary sharp maxima (Fig. 5c) as a result of a very high state of crystalline orientation. After intermediate deformation ratios, most of the material is well-oriented, but there is still a significant amount of randomly-oriented crystals, shown by the background ring upon which the diffraction maxima are superimposed (Fig. 5b). Above a deformation ratio of 5, no randomly-oriented crystals could be detected. These observations show that the deformation process is non-affine since affine deformation would simply cause a gradual reduction in angular width of each reflection. The randomly-oriented crystals present after relatively large deformations could be present as small "islands" in a uniformly-oriented structure. Such islands have been observed using optical microscopy and are probably present because of the non-uniform manner in which the spherulitic structure is deformed [12].

4.4. Crystalline orientation functions

The presence of randomly oriented crystals, as discussed above, for deformation ratios up to 5, was detected in the texture diffractometer scans as a constant shift from the baseline. Because the actual baseline has to be measured independently, quantitative estimation of the amount of randomly-oriented crystals is subject to considerable error.

The peaks in the diffractometer scans for both highly-oriented and slightly-oriented samples were shown to be gaussian. In all cases, therefore, the orientation functions could be determined by computation using the standard deviation estimated from the width at half peak height. This of course neglects the randomly-oriented crystals which are present at low deformation ratios. The results differ considerably at low deformation ratios from those calculated including the random crystals and their precision is much greater. Results both including and excluding the random crystals are likely to be significant and either could relate to mechanical properties. For this reason both were measured and will be discussed.

The variation of $\overline{\sin^2 \theta}$ with deformation ratio (Fig. 6) indicates that most crystalline orientation has occurred during deformations up to a ratio of 5. Larger deformations produce only very small increases in orientation.

Values of the average crystalline orientation function $\overline{\sin^2 \theta}$, calculated from the entire diffractometer scans including random crystals, agree to a first approximation with values for $\overline{\sin^2 \theta}$ calculated from birefringence using Equation 1. A small systematic difference, as indicated by the results shown in Fig. 7, is to be expected since birefringence is influenced by molecular segments in non-crystalline regions as well as those in a crystal lattice. There could also be a "form birefringence" term [13]. The birefringence of a polymer is sometimes considered to consist of two separate components: one due to the crystalline regions and one due to the disordered regions. The difference between X-ray

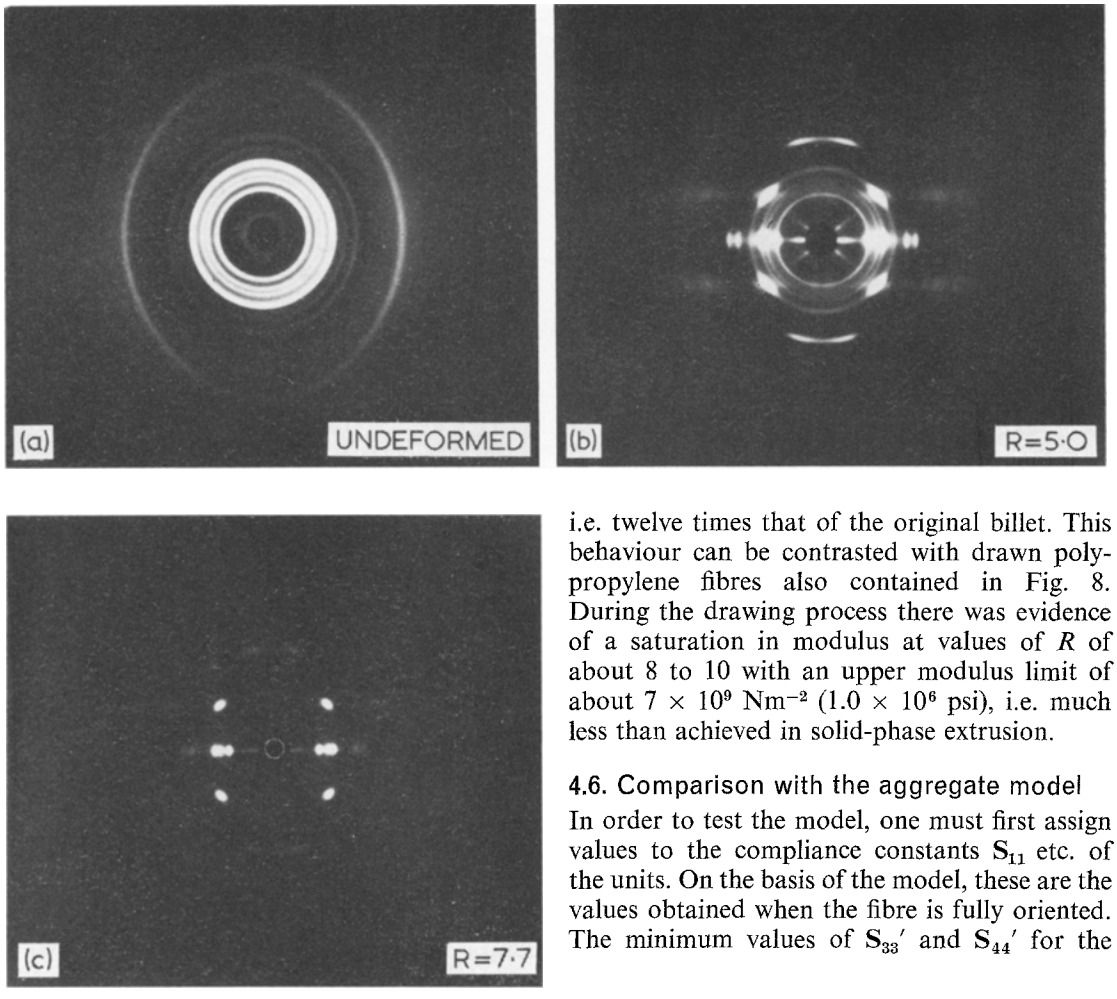

Figure 5 Wide-angle X-ray diffraction patterns of extrudate (extrusion direction vertical) (a) original billet (undeformed) (b) deformation ratio $R = 5$ (c) $R = 7.7$.

and birefringence data (indicated in Fig. 7) can then be used to quantitatively estimate the disordered contribution to birefringence if allowance is made for form birefringence [13].

4.5. Tensile modulus

With increase in deformation ratio R, the tensile modulus of the extrudate increased (Fig. 8). At small values of R the rate of increase of modulus was relatively small, but above a value of about 5, a dramatically large constant rate of increase was observed. The linear modulus increase continues up to the largest obtainable deformation ratio ($R = 15$). At this deformation the value achieved was 1.7×10^{10} Nm^{-2} (2.4×10^6 psi), i.e. twelve times that of the original billet. This behaviour can be contrasted with drawn polypropylene fibres also contained in Fig. 8. During the drawing process there was evidence of a saturation in modulus at values of R of about 8 to 10 with an upper modulus limit of about 7×10^9 Nm^{-2} (1.0×10^6 psi), i.e. much less than achieved in solid-phase extrusion.

4.6. Comparison with the aggregate model

In order to test the model, one must first assign values to the compliance constants S_{11} etc. of the units. On the basis of the model, these are the values obtained when the fibre is fully oriented. The minimum values of S_{33}' and S_{44}' for the

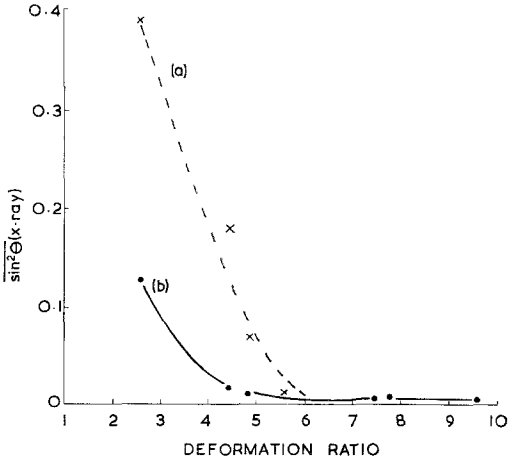

Figure 6 Variation in the X-ray orientation function $\overline{\sin^2\theta}$ with deformation ratio (a) including and (b) neglecting randomly oriented crystals.

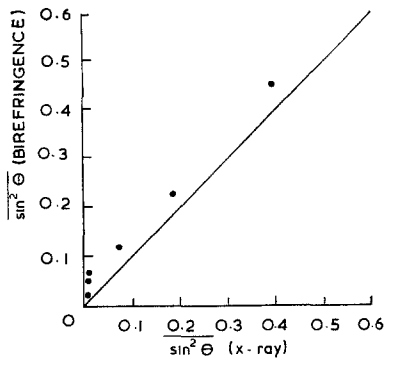

Figure 7 Comparison of X-ray and birefringence orientation functions. If the functions for each sample were equal, each point would lie on the straight line drawn.

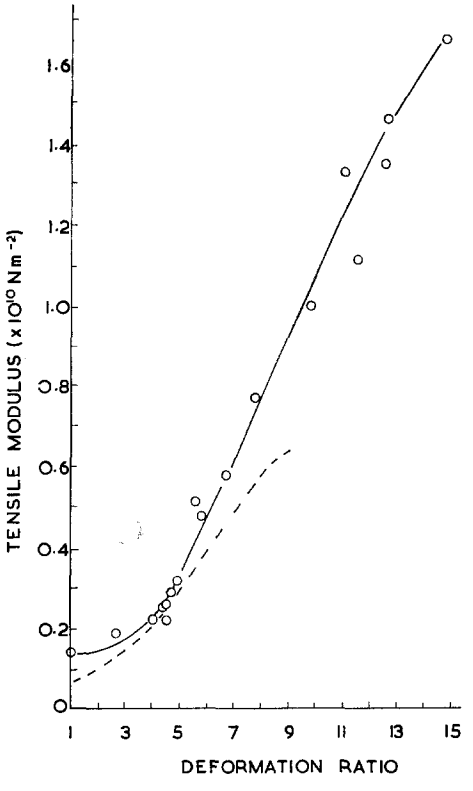

Figure 8 Variation of extrudate tensile modulus with deformation ratio. Dotted curve shows previous results for cold-drawn polypropylene fibres [6].

extrudate were therefore selected. Values for S_{11} and S_{12} were obtained from transverse compressional measurements on the high deformation ratio cylindrical extrudate [14]. Poissons ratio ν_1 for highly oriented extrudate

TABLE I Compliances for polypropylene units of structure

Material	Compliance constants ($\times 10^{-10}$ m^2 N^{-1})				
	S_{11}	S_{33}	S_{44}	S_{13}	S_{12}
Hydrostatically-extruded	10.9	0.59	8.4	−0.22	−10.8
Drawn fibres	12.8	1.0	12.5	−0.50	−6.6

with axial stresses has been measured at 0.37 [14, 15] and hence S_{13} ($= \nu_1 S_{33}$) was calculated. S_{12} was calculated in similar manner from measurements [14] of the transverse Poissons ratio. The selected values for the constants are summarized in Table I, together with values deduced previously for the units of polypropylene fibres. Differences between the two sets result from the higher ultimate moduli observed for extrudate. The one inconsistency in the selected constants for extrudate and fibres is in the constant S_{12}. It was pointed out previously, however, that the fibres value was unreasonable [6], and this value was only selected in order to give a fit between the aggregate model and the fibre torsional compliance.

The matrix inversion formulae used to predict the stiffness constants for the Voigt bound involve the expression $(S_{11} + S_{12})$ [16]. Because $-S_{12}$ is very close to S_{11}, this is a very small number which cannot be determined very accurately. It is therefore only possible to define an approximate trend for this upper bound.

A comparison between experimentally-observed compliances and those calculated using the aggregate model is shown in Figs. 9 and 10. For the Reuss bound, two theoretical curves have been drawn one using orientation functions calculated including the randomly oriented crystals present for deformation ratios up to 5 and the other neglecting these crystals. The best fit between experimental results and the theory is obtained using the Reuss (lower) bound and including the randomly oriented crystals. Even in this case, however, at intermediate deformation ratios the predicted extensional compliances are too small. In addition the changes in the orientation functions for deformation ratios above 5 are much too small to predict the experimentally-observed decrease in compliance in this region. The latter discrepancy is more serious than at first apparent in Fig. 9 since the steady decrease in compliance corresponds to a very

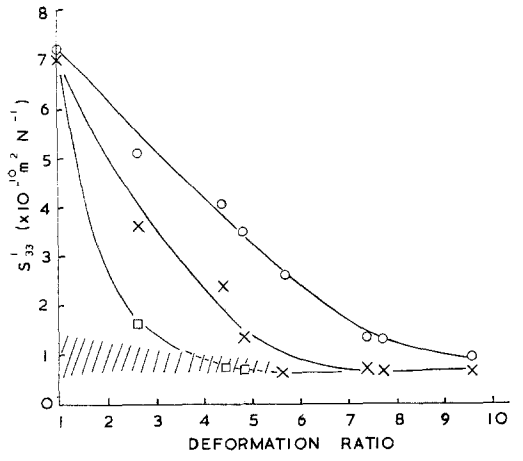

Figure 9 Comparison of experimental and theoretical extensional compliances. Experimental points are marked O. Theoretical values were calculated from the aggregate model in three different ways: point X from the Reuss bound including random crystals, points □ from the Reuss bound neglecting random crystals, and the shaded area shows the approximate region of theoretical Voigt bound.

large increase in modulus which is not predicted experimentally. The continuing decrease in compliance at large deformation ratios must be due to structural changes in addition to simple re-orientation of basic units. In terms of the model this would correspond to changes in the compliance constants of the basic units of structure. Now for comparison with the theory, compliance constants for the units were predicted from the ultimate extrudate modulus. A better fit to the theory at low deformation ratios would be obtained by using larger compliance constants for the units. For example if S_{33} was taken as 2.5×10^{-10} m^2 N^{-1} then the Reuss curve would fit the experimental results of Fig. 9 up to a deformation ratio of 5. Above this ratio the decrease in compliance would correspond to a steady reduction in the effective extensional compliance constant of the unit.

For the torsional compliance, it will be noted that the results do not fit close to the Reuss bound, although this bound does predict the correct trend with deformation ratio. It is not unreasonable, however, for uniform stress conditions to hold for one mode of deformation and not for another mode. A decrease in unit compliance constants with increase in deformation ratio above 5 is again necessary for experimental results to lie between the upper and lower bounds at all deformation ratios.

4.7. Low-angle X-ray diffraction

A Franks camera was used to obtain low angle X-ray diffraction patterns for sections cut from the extrudate. The uniform ring of the isotropic original billet was replaced by an arc with maximum intensity on the meridian (i.e. in the deformation direction) after small deformation ratios. Increase in the deformation ratio up to a value of 5 reduced the width of the arc indicating that the crystal surfaces were becoming more highly oriented in planes perpendicular to the deformation direction. The periodicity was constant at 189 ± 5 Å. For deformation ratios above 5, much more complex structural changes were indicated. The reflections

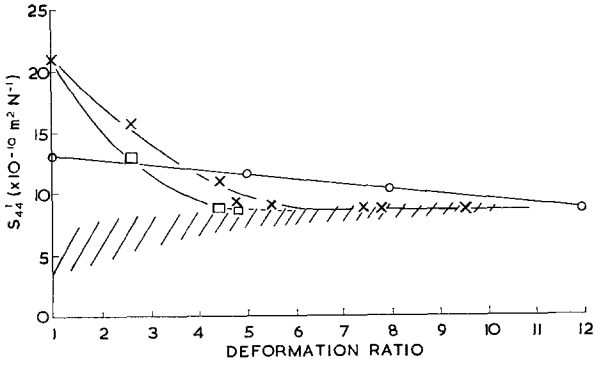

Figure 10 Comparison of experimental and theoretical torsional compliances. Experimental points are marked O. Theoretical values were calculated from the aggregate model in three ways: point X from the Reuss bound including random crystals, points □ from the Reuss bound neglecting random crystals, and the shaded area shows the approximate region of the theoretical Voigt bound.

broadened in a direction perpendicular to the meridian and formed a layer-line pattern as is frequently observed for cold-drawn polymers. In addition, an extra reflection became apparent on the equator, i.e. corresponding to a structural regularity perpendicular to the deformation direction. The deduced periodicity of this extra reflection was 45 Å. Its origin is at present not known. It is interesting to compare the low-angle X-ray measurements with the discussion of the applicability of the aggregate model. For deformation ratios up to 5, simple lamella re-orientation is consistent with both sets of data. The complex low-angle X-ray diffraction changes occurring above a deformation ratio of 5 and the large increase in modulus which occurs in this region could be related. It is for this reason that the low-angle X-ray diffraction data has been mentioned in this paper. More detailed measurement and discussion of the diffraction patterns will be made later [17].

4.8. Dynamic mechanical data

Torsion pendulum measurements of torsional modulus (τ) and tan δ as a function of temperature (Fig. 11) show complicated features. At temperatures below 0°C the unoriented sample has the largest modulus. There is a reversal in torsional stiffnesses accompanying the loss process at 0 to 10°C and at room temperature, τ increases with deformation ratio. A reversal could be caused simply by the temperature causing the stress state in the sub-units to move towards the uniform strain condition with decrease in temperature. Alternatively, one could consider that there might be two different modes of deformation, one in operation well above room temperature and the other well below room temperature. It is obvious therefore that for a full understanding of the relationship between structure and mechanical properties of solid-phase extruded polymers, a long, detailed scientific investigation will be necessary.

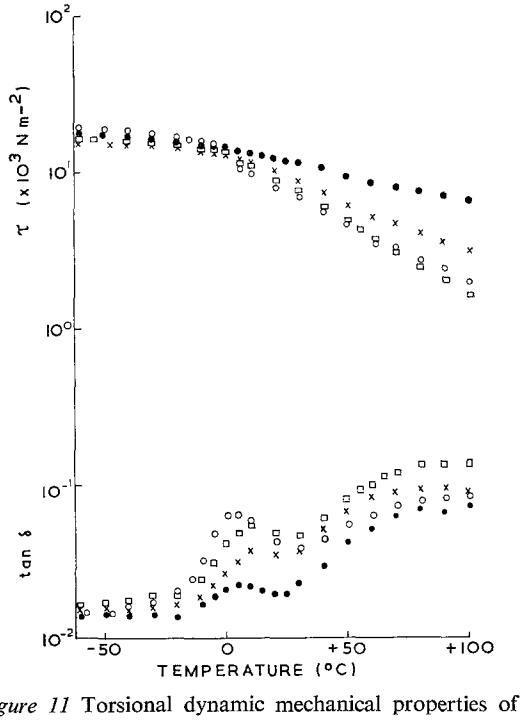

Figure 11 Torsional dynamic mechanical properties of extrudate: (O) original billet; (□) deformation ratio $R = 5$; (X) $R = 8$; (●) $R = 12$.

5. Conclusions

It has been shown that application of the metal-shaping technique solid-phase hydrostatic extrusion to plastics gives rods of high uniaxial orientation. As in the case of fibres and films, this molecular orientation causes large increases in stiffness. Indeed solid-phase extruded polypropylene has a larger modulus after a given deformation than drawn polypropylene fibres. In addition, higher deformations can be achieved and hence the ultimate modulus obtainable is much larger using solid-phase extrusion.

Birefringence measurements have demonstrated that the orientation variation across sections of extrudate is surprisingly small, even for complicated extrusion flow patterns. This is thought to be due to the increased resistance to yielding of the material following deformation. A strained element therefore resists further strains until neighbouring elements have been equally deformed.

Both birefringence and wide-angle X-ray diffraction indicate that deformation is non-affine. The latter technique shows that even when most crystals have been well-oriented there are still a small number of randomly-oriented crystals.

At low deformation ratios, the variation in modulus with orientation is not inconsistent with a simple aggregate model, provided a suitable choice of compliance constants for the units of structure is made. The large increase in modulus at large deformation ratios cannot, however, be explained by this model and changes in structure other than simple re-orientation

must be involved. Complicated structural changes for deformation ratios above 5 are also indicated by low-angle X-ray diffraction patterns.

Acknowledgements

Solid-phase extrusion has been studied in ICI by a team of scientists (C. Cassin, A. G. Gibson, G. Allcock, J. B. Bunney, R. Hughes, R. Murray, G. D. Wignall, G. Longman and the author) and the author is extremely indebted to all of them for their helpful comments and advice throughout the course of this work. He is also extremely indebted to Professor I. M. Ward of Leeds University, England for many useful suggestions and discussions. Some low-angle X-ray diffraction measurements were carried out at Leeds University by Dr R. A. Duckett.

Appendix

Evaluation of *c*-axis orientation distribution from measured orientation distribution of the normals of two planes containing the *c*-axis

The *c*-axis orientation distribution has been calculated from the measured orientation distributions of normals to two planes containing the *c*-axis using an expression quoted by Wilchinsky [9]. Since the proof of the expression is not available, it was thought to be desirable to derive it independently and this is done in this Appendix.

Let $X^1Y^1Z^1$ be a set of rectangular Cartesian co-ordinates fixed in the sample. $\hat{Z}^1$ is the reference direction which is an axis of symmetry.

Let $X\ Y\ Z$ be a set of rectangular Cartesian co-ordinates fixed in an individual crystal. ($\hat{Z}$ is the direction of the normal to the set of planes whose distribution about $\hat{Z}^1$ is required.)

Let θ be the angle between $\hat{Z}$ and $\hat{Z}^1$.

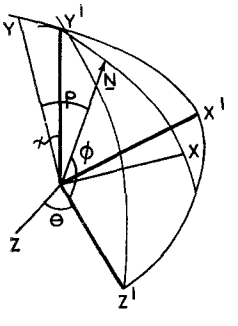

Figure A1 Geometrical relationship between axes $X^1\ Y^1Z^1$ fixed in the sample (Z' being the deformation direction) and a set XYZ fixed in an individual crystalline unit.

Now $\hat{Z}^1$ is an axis of symmetry for the sample, therefore axes X^1Y^1 can be rotated about $\hat{Z}^1$ and X^1 can be fixed in the ZZ^1 plane (see Fig. A1). For this case, $\hat{Y}^1$ is perpendicular to $\hat{Z}$ and $\hat{Z}^1$, and therefore lies in the XY plane.

Consider a set of planes (normal $\hat{N}$) which contains the $\hat{Z}$ axis; $\hat{N}$ is perpendicular to Z. Thus $\hat{N}$ is in the YY^1X plane.

The angle between $\hat{N}$ and $\hat{Y}$, ρ, is defined by the crystalline structure.

The angle between $\hat{N}$ and $\hat{Z}^1$, ϕ is measured.

With respect to XYZ-axes (which have unit vectors $i\,j\,k$),

$$\hat{N} = \sin\rho\, i + \cos\rho\, j \qquad \text{(Ai)}$$

and

$$\hat{Z}^1 = \sin\theta\cos\chi i - \sin\theta\sin\chi j + \cos\theta k \qquad \text{(Aii)}$$

Now,

$$\cos\phi = \hat{N}\,.\,\hat{Z}^1 = \sin\rho\sin\theta\cos\chi - \sin\theta\sin\chi\cos\rho \qquad \text{(Aiii)}$$

$$\therefore \cos^2\phi = \sin^2\rho\sin^2\theta\cos^2\chi + \cos^2\rho\sin^2\theta\sin^2\chi - 2\sin\rho\cos\rho\sin\chi\cos\chi\sin^2\theta \qquad \text{(Aiv)}$$

If χ^1 is the angle between the projection of Y on the X^1Y^1 plane and the Y^1 direction, then:

$$\cos\chi = \cos\chi^1\cos\theta$$

Therefore

$$\cos^2\chi = \cos^2\chi^1\cos^2\theta$$

and

$$\sin^2\chi = 1 - \cos^2\chi^1\cos^2\theta$$

Equation (Aiv) therefore becomes

$$\cos^2\phi = (\sin^2\rho - \cos^2\rho)\cos^2\chi^1\sin^2\theta\cos^2\theta + \cos^2\rho\sin^2\theta - 2\sin\rho\cos\rho\sin^2\theta\cos\theta\cos\chi^1\sqrt{(1-\cos^2\chi^1\cos^2\theta)} \qquad \text{(Av)}$$

There is no preferred orientation of the crystals in a plane perpendicular to $\hat{Z}^1$. This means that any crystal direction, e.g. the Y-axis of the crystal will not be preferentially oriented in the X^1Y^1 plane. χ^1 is therefore independent of θ. Thus averaging for all crystals:

$$\overline{\cos^2\chi^1\sin^2\theta\cos^2\theta} = \overline{\cos^2\chi^1}\ \overline{\sin^2\theta\cos^2\theta} = \tfrac{1}{2}\overline{\sin^2\theta\cos^2\theta}$$

and

$$\sin^2\theta\cos\theta\cos\chi^1\sqrt{(1-\cos^2\chi^1\cos^2\theta)} = 0$$

Averaging (Av) for all crystals for a plane $\hat{N}_1$ with $\phi = \phi_1$ and $\rho = \rho_1$

$$\overline{\cos^2\phi_1} = \tfrac{1}{2}(\sin^2\rho_1 - \cos^2\rho_1)\,\overline{\sin^2\theta\cos^2\theta} + \cos^2\rho_1\,\overline{\sin^2\theta} \qquad \text{(Avi)}$$

For a plane $\hat{N}_2$ with $\phi = \phi_2$ and $\rho = \rho_2$

$$\overline{\cos^2\phi_2} = \tfrac{1}{2}(\sin^2\rho_2 - \cos^2\rho_2)\,\overline{\sin^2\theta\cos^2\theta} + \cos^2\rho_2\,\overline{\sin^2\theta} \qquad \text{(Avii)}$$

From (Avi) and (Avii)

$$\overline{\sin^2\theta} = \frac{(\sin^2\rho_2 - \cos^2\rho_2)\,\overline{\cos^2\phi_1} - (\sin^2\rho_1 - \cos^2\rho_1)\,\overline{\cos^2\phi_2}}{\cos^2\rho_1\sin^2\rho_2 - \cos^2\rho_2\sin^2\rho_1}$$

Thus,

$$\overline{\cos^2\theta} = 1 - \frac{(1 - 2\sin^2\rho_2)\,\overline{\cos^2\phi_1} - (1 - 2\sin^2\rho_1)\,\overline{\cos^2\phi_2}}{\sin^2\rho_1 - \sin^2\rho_2} \quad \text{(Aviii)}$$

Eliminating $\overline{\sin^2\theta}$ from (Avi) and (Avii) gives

$$\overline{\sin^2\theta\cos^2\theta} = \frac{2\cos^2\rho_2}{\sin^2\rho_1 - \sin^2\rho_2}\,\overline{\cos^2\phi_1} - \frac{2\cos^2\rho_1}{\sin^2\rho_1 - \sin^2\rho_2}\,\overline{\cos^2\phi_2} \quad \text{(Aix)}$$

References

1. G. C. OPPENLANDER, *Science* **159** (1968) 1311.
2. A. PETERLIN, *J. Polymer Sci.* **C9** (1965) 61.
3. I. M. WARD, *Proc. Phys. Soc.* **80** (1962) 1176.
4. V. B. GUPTA and I. M. WARD, *J. Macromol. Sci.* **B1** (1967) 373.
5. P. R. PINNOCK and I. M. WARD, *Brit. J. Appl. Phys.* **15** (1964) 1559.
6. *Idem, ibid*, **17** (1966) 575.
7. H. U. D. PUGH and A. H. LOW, *J. Inst. Metals* **93** (1964-5) 201.
8. L. R. G. TRELOAR, *Plastics and Polymers* **39** (1971) 29.
9. Z. W. WILCHINSKY, *J. Appl. Phys.* **30** (1959) 792; **31** (1960) 1969.
10. C. CASSIN, to be published.
11. L. E. ALEXANDER, "X-ray Diffraction Methods in Polymer Science" (Wiley, New York, 1969).
12. I. L. HAY and A. KELLER, *Kolloid Z.u.Z.f. Polymere* **204** (1965) 43.
13. F. BETTLHEIM and R. STEIN, *J. Polymer Sci.* **27** (1958) 567.
14. I. M. WARD, unpublished data.
15. J. B. BUNNEY, unpublished data.
16. H. BRODY and I. M. WARD, *Polymer Eng. Sci.* **11** (1971) 139.
17. R. A. DUCKETT and I. M. WARD, to be published.

Received 3 May and accepted 30 June 1972.